Structure and Synthesis of SSZ-63: Toward an Ordered Form of Zeolite Beta

Allen W. Burton,* Saleh Elomari,* Ignatius Chan, Ajit Pradhan, and Charles Kibby

ChevronTexaco Energy Research and Technology Company, Richmond, California 94802

Received: May 10, 2005; In Final Form: August 22, 2005

The synthesis, characterization, and structure elucidation of the borosilicate zeolite SSZ-63 are described. SSZ-63 is synthesized using the 1-cyclodecyl-1-methylpyrrolidinium cation as a structure-directing agent. The structural model for SSZ-63 was determined by comparison of its powder X-ray diffraction pattern with those of zeolite beta and its polytype structures. Whereas conventional zeolite beta may be described as a random intergrowth of polytypes A and B, SSZ-63 is more accurately described as a random intergrowth of polytypes B and C_H (the hypothetical polytype C proposed by Higgins). Polytype C_H is essentially an ordered intergrowth (of polytypes A and B) in which one of the crystallographic projections is equivalent to those in polytype A and another projection is equivalent to those in polytype B. Unlike zeolite beta, which possesses significant disorder related to layer shifts along both the *a*- and *b*-crystallographic axes, the structure of SSZ-63 has little disorder associated with the translations of layers in the *a*-direction. DIFFaX simulations of the powder diffraction patterns, electron diffraction, and high-resolution transmission electron microsocopy data all support the proposed model.

I. Introduction

Zeolite beta has been known since the 1960s, when it was first prepared by researchers at Mobil using the tetraethylammonium ion.[1] In addition to tetraethylammonium, many other organic molecules have since been reported as structure-directing agents for zeolite beta.[2] A naturally occurring form of zeolite beta, tschernischite, was reported in 1993.[3] Since the elucidation of the beta structure, researchers have strived to prepare ordered polytypes of zeolite beta, particularly the chiral polytype A (vide infra).

Zeolite beta possesses a three-dimensional system of pores that are delimited by 12-ring windows. Models for the structure of zeolite beta were presented independently first by Higgins and co-workers[4] and Newsam and co-workers.[5] Zeolite beta is a heavily faulted material that is formed by the epitaxial stacking of the layer shown in Figure 1. The layers stack in a direction parallel to the 2-fold axis of each layer. For simplicity we will refer to this direction as the "*c*-axis" in the description of each pure polytype as well as the disordered models. Six end polytypes of zeolite beta may be formed depending upon the stacking arrangements of the layers. Panels a−c of Figure 2 present the different projections (along a single-crystal axis, the [100] axis) that are found in these pure polytypes. In the case shown for Figure 2a, every other layer stacks in an alternating sequence of $+^1/_3b$ then $-^1/_3b$ relative to its preceding layer. Note that the layers between these layers cannot be shifted along the *b*-direction; however, these "in-between" layers may be shifted either $+^1/_3a$, 0*a*, or $-^1/_3a$ without changing the projection along the [100] axis. In Figure 2b, the translations are always in the same direction (only $+^1/_3b$ or only $-^1/_3b$), whereas in Figure 2c there are no translations along the *b* axis. Note that the projection of the pore windows will appear as an ABAB, ABCABC, or AAAA arrangement in the cases of panels a, b, and c, respectively, of Figure 2.

When there is a strictly alternating stacking sequence of every other layer along projections of both crystal axes (i.e., $+^1/_3a$, $-^1/_3a$ along the *b*-projection and $+^1/_3b$, $-^1/_3b$ along the *a*-projection), the polytype is called "A". Note that polytype A actually represents two different structures depending upon whether the sequence of layers stacks ($+^1/_3a$, $+^1/_3b$, $-^1/_3a$, $-^1/_3b$) or ($+^1/_3a$, $-^1/_3b$, $-^1/_3a$, $+^1/_3b$). One model has $P4_122$ space group symmetry, whereas the other has $P4_322$ symmetry. Since the models differ only in the handedness of the 4-fold screw axis, they are chiral enantiomorphs of one another.

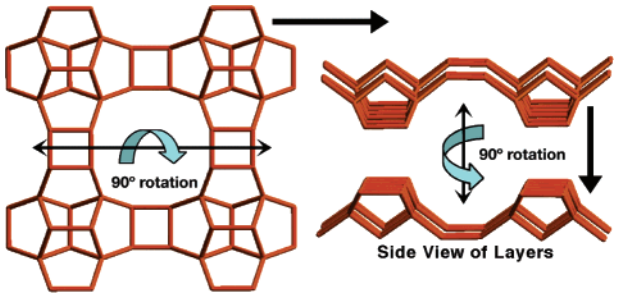

Figure 1. Layer that epitaxially stacks to form the polytype structures of zeolite beta. The oxygen atoms have been omitted from the structure for clarity, and bonds have been placed between neighboring silicon atoms.

If the stacking sequence of every other layer is always in the same direction when viewed along both projections (i.e., either always $+^1/_3b$ or always $-^1/_3b$ along the *bc* projection, and either always $+^1/_3a$ or always $-^1/_3a$ along the *ac* projection), the polytype is called "B".

The polytype which possesses no translations in either the *a*- or *b*-direction has been designated "C" by Newsam et al. Note that for polytypes A and B, the ring features and local bond angles are very similar. Their projections can both be constructed from the familiar 5^46^1 "butterfly unit", and the connectivity of the chains of butterfly units within the plane of the projection differs by only a mirror plane or a translational symmetry operation for polytype A or B, respectively. The structural and energetic similarities[6] in the pure polytypes are probably responsible for the difficulty in preparing either of these two pure endmembers. In contrast, the projection of

10.1021/jp052438x CCC: $30.25
Published on Web 10/06/2005

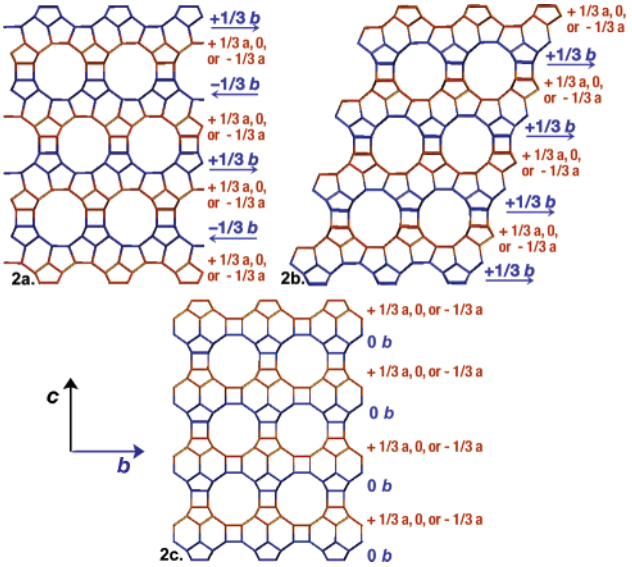

Figure 2. Two-dimensional projections along a single axis that demonstrate the stacking sequences of layers observed in (a) polytype A, (b) polytype B, and (c) polytype C of zeolite beta.

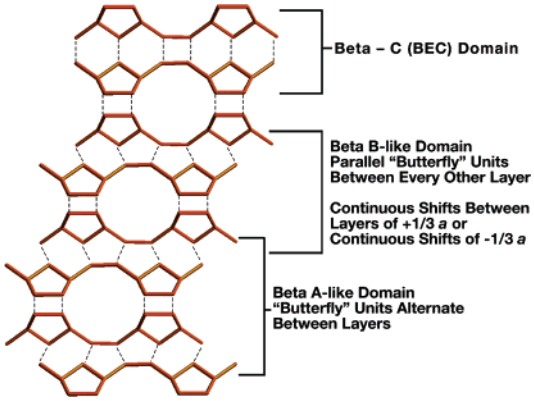

Figure 3. Projection of a fragment of a hypothetical beta structure showing the different stacking vectors that may occur. The bonds between the layers are indicated by dashed lines.

polymorph C is composed of $6^2 5^2$ ring units that are connected by four-ring units. The different ring features give rise to local bond angles and channel features that are disparate from those in polytypes A and B. Most notably, polymorph C possesses a high density of double four-ring units that usually are not observed in highly siliceous zeolites prepared in non-fluoride media. Corma and co-workers have prepared pure polytype C and beta intergrowths with varying degrees of C "character" by using different Si/Ge ratios in their synthesis gels.[7] The longer Ge−O bond lengths are more amenable to the angles required for the double four-ring units. Camblor et al. have likewise prepared beta polymorphs with varying degrees of C intergrowth by using fluoride in all-silica systems.[8]

Other polytypes can be constructed by requiring different stacking schemes within the *ac* and *bc* faces. For example, a strictly alternating $+^1/_3$, $-^1/_3 b$ stacking arrangement of every other layer within the *bc* face and a permanent stacking arrangement of $+^1/_3 a$ (or equivalently $-^1/_3 a$) within the *ac* face yields a polytype designated C by Higgins et al. To avoid confusion with the polytype C defined by Newsam, we will refer to this framework as polytype C_H. Polytype C_H is essentially an ordered intergrowth (of polytypes A and B) in which one of the crystallographic projections is equivalent to those in polytype A, and another projection is equivalent to those

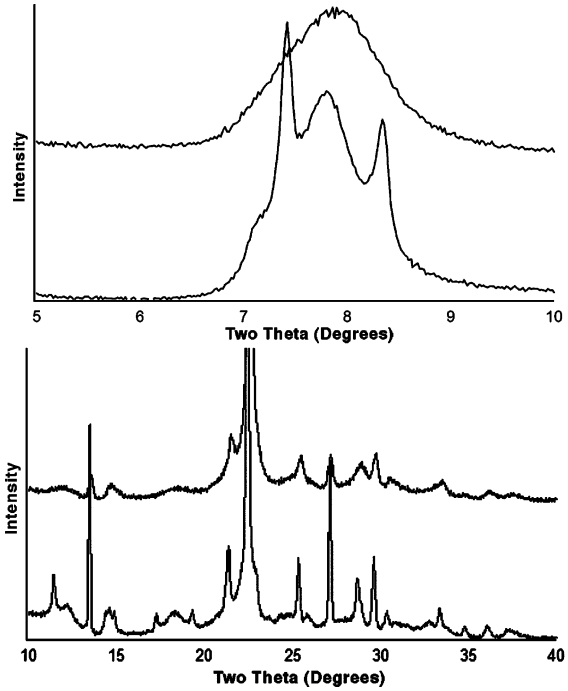

Figure 4. Comparison of the powder X-ray diffraction patterns (Cu Kα radiation) of (top) zeolite beta and (bottom) SSZ-63.

TABLE 1: Chemical and Physical Data for SSZ-63

C/H/N of as-made zeolite from combustion analysis	
C wt %	15.38
H wt %	2.62
N wt %	1.19
atomic ratios	15.1C:30.6H:1N
Si wt %	33.47
B wt %	0.33
atomic ratios	39Si:1B
organic content of as-made zeolite from TGA (%)	19.2
water content of as-made zeolite from TGA (%)	2.0
argon micropore volume (cm^3/g)	0.22
nitrogen micropore volume (cm^3/g)	0.24

in polytype B. Likewise, polytype D possesses no translations of layers along the *ac* face and a permanent stacking arrangement of $^1/_3 b$ (or $-^1/_3 b$) along the *bc* face. Polytype E possesses no translations of layers along the *ac* face and a strictly alternating $+^1/_3$, $-^1/_3 b$ stacking arrangement of every other layer along the *bc* face.

The polytypes described above define all possible end-members of zeolite beta that have ordered and independent stacking sequences within both the *a* and *b* directions. Any framework that is formed by a random or nonrandom stacking sequence of the layer illustrated in Figure 1 is defined to be a beta polymorph. Figure 3 shows a short fragment of such a hypothetical disordered zeolite. With the exception of polytype C, none of the pure polytypes has been observed experimentally.

A typical powder X-ray diffraction pattern of zeolite beta is shown in the tops of Figure 4. Note that the pattern is characterized by several severely broadened peaks and some relatively sharp Bragg reflections. The sharp reflections in the pattern can be indexed in the tetragonal cell of polytype A with $a = 12.47$ and $c = 26.33$ Å.[9] Higgins et al. and Newsam et al. noted that for *hkl* reflections where $h \neq 3n$ or $k \neq 3n$, the diffraction peaks were diffuse or very weak whereas for

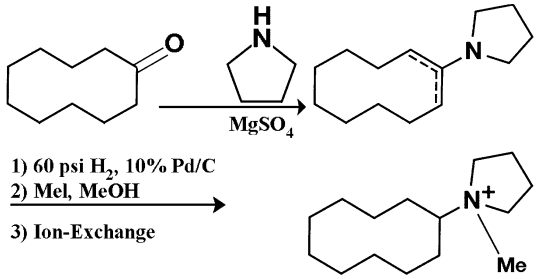

Figure 5. Synthetic procedure used to prepare the structure-directing agent for SSZ-64.

reflections in which both $h = 3n$ and $k = 3n$, the corresponding peaks were sharp (note that n denotes an arbitrary integer that may have a different value for h and k in a given reflection). The structural disorder was likewise manifested in the electron diffraction pattern along ⟨010⟩ . For a typical zeolite beta, the electron diffraction pattern along ⟨100⟩ will be indistinguishable from the ⟨010⟩ diffraction pattern. In contrast, although no streaking can be observed in the ⟨001⟩ electron diffraction pattern (because the streaking is along c^*), the peaks for which $h \neq 3n$ or $k \neq 3n$ are extremely weak.

The streaking observed in the electron diffraction (and the broadening observed in the powder diffraction pattern) is characteristic of a material that has stacking disorder along the c-axis. Since the peaks for which h or $k \neq 3n$ are diffuse, this means these layers are related by random translational shifts of either $\pm^1/_3a$ or $\pm^1/_3b$. From these considerations, the investigators derived the pure polytype models.

In a landmark publication for zeolite science, Newsam et al. confirmed their proposed model and determined the approximate degree of stacking disorder for zeolite beta. This work introduced the DIFFaX program[10] for the simulation of powder diffraction patterns of materials that may be described by intergrowths of specified atomic layers. The program requires the atomic coordinates of each layer, the stacking vectors relating each layer type, and the stacking probability of one layer type to another. By performing a series of pattern simulations for different fault probabilities, Newsam determined that zeolite beta has about 43% polytype A and 57% polytype B character. This implies that in conventional samples of zeolite beta, there is a nearly equal probability of a layer translation of $+^1/_3u$ or $-^1/_3u$ relative to the second previous layer (where u is either a or b). Because many zeolites are faulted materials (including elucidated or undetermined frameworks), the introduction of DIFFaX has allowed the verification of proposed models for many disordered zeolite structures.[11−18]

In this work we describe the synthesis and characterization of SSZ-63. Unlike conventional zeolite beta, SSZ-63 is more accurately described as a random intergrowth of polytypes B and C_H rather than polytypes A and B. Although SSZ-63 possesses a faulted structure, SSZ-63 represents a more well-ordered form of zeolite beta.

II. Experimental Methods

Synthesis of the Structure-Directing Agent. The structure-directing agent (SDA), 1-cyclodecyl-1-methylpyrrolidinium (CDMP) cation, was synthesized according to the procedure described below (see Figure 5). Cyclodecanone (25 g, 0.16 mol) was added to 320 mL of anhydrous hexane in a three-neck round reaction bottom flask equipped with a reflux condenser and an overhead mechanical stirrer. Pyrrolidine (34 g, 0.48 mol) and 48 g (0.4 mol) of anhydrous magnesium sulfate were then added to the solution. The resulting mixture was stirred while heating at reflux for 5 days. The reaction mixture was filtered through a fritted-glass funnel. The filtrate was concentrated at reduced pressure on a rotary evaporator to yield 32 g (96%) of the expected enamine (1-cyclodec-1-enylpyrrolidine) as a reddish oily substance. ^{1}H NMR and ^{13}C NMR spectra were consistent with the desired product. The enamine was dissolved in ethanol and reduced to the corresponding amine (1-cyclodecyl-pyrrolidine) in quantitative yield via catalytic hydrogenation in the presence of 10% Pd on activated carbon at a hydrogen pressure of 65 psi. To a solution of 30 g (0.14 mol) of 1-cyclodecyl-pyrrolidine in 250 mL of anhydrous methanol in a 1 L reaction flask was added 30 g (0.21 mol) of methyl iodide. The reaction mixture was mechanically stirred for 48 h at room temperature. Then, an additional 0.5 molar equiv of methyl iodide was added, and the mixture was refluxed for 30 min. The reaction mixture was cooled and concentrated under reduced pressure on a rotary evaporator to give the product as a pale yellow solid material. The product was purified by dissolving in acetone and then precipitating by adding diethyl ether. CDMP iodide was obtained as a white powder in 93% yield (46 g, ^{1}H NMR and ^{13}C NMR were ideal for the iodide salt).

The hydroxide version of CDMP was obtained by ion exchange of the iodide according to the procedure below. 1-Cyclodecyl-1-methylpyrrolidinium iodide (45 g, 0.128 mol) was dissolved in 150 mL of water in a 500 mL plastic bottle. To this solution was added 160 g of ion-exchange resin-OH (BIO-RAD AH1-X8), and the mixture was gently stirred at room temperature overnight. The mixture was filtered, and the solids were rinsed with an additional 85 mL of water. The reaction afforded 0.12 mol of the SDA in the hydroxide form as indicated by titration analysis with 0.1 N HCl.

Zeolite Synthesis. SSZ-63 was synthesized hydrothermally by heating a mixture of CAB-O-SIL M-5 (SiO_2 source), sodium borate decahydrate, aqueous hydroxide solution of CDMP, sodium hydroxide, and water. The molar ratios were 0.1 SDA_2O: 0.05 Na_2O:0.022 B_2O_3:45 H_2O:1.0 SiO_2. The reaction mixture was then heated at 160 °C (±1 °C) with tumbling at about 43 rpm. The synthetic procedure below is a representative example for making the borosilicate version of SSZ-63.

First, 5.88 g of a 0.51 M aqueous solution of CDMP hydroxide (3 mmol of SDA), 1.2 g of a 1 M aqueous solution of NaOH (1.2 mmol of NaOH), and 5.1 g of deionized water were added to a 23 cm^3 Teflon liner. To this mixture was added 0.062 g of sodium borate decahydrate (0.157 mmol of $Na_2B_4O_7$•$10H_2O$; ∼0.65 mmol of boron), and the mixture was stirred until completely dissolved. To this solution was added 0.9 g of CABO-SIL M-5 fumed silica (∼14.7 mmol of SiO_2), and the mixture was thoroughly stirred (by hand) using a Teflon spatula. The resulting gel was capped off and placed in a Parr steel autoclave and heated in an oven at about 160 °C (±1 °C) while tumbling at about 43 rpm. The reaction was monitored by periodically monitoring the pH of the gel, and by looking for crystal growth using scanning electron microscopy (SEM). After being heated for 12 days, the starting reaction gel turned into a clear liquid layer and a fine powdery precipitate. The mixture was filtered through a fritted-glass funnel, and the collected solids were thoroughly washed with water (∼1 L) and rinsed with acetone (∼40 mL) to remove any organic residues. The solid product was dried in open air overnight, and further dried in an oven at 120 °C for 3 h. The reaction afforded 0.88 g of SSZ-63 as determined by powder X-ray diffraction (XRD) analysis. The structure-directing agent was removed from the zeolite channels by slow calcination to 595 °C in a nitrogen atmosphere with ∼2% oxygen bled in.

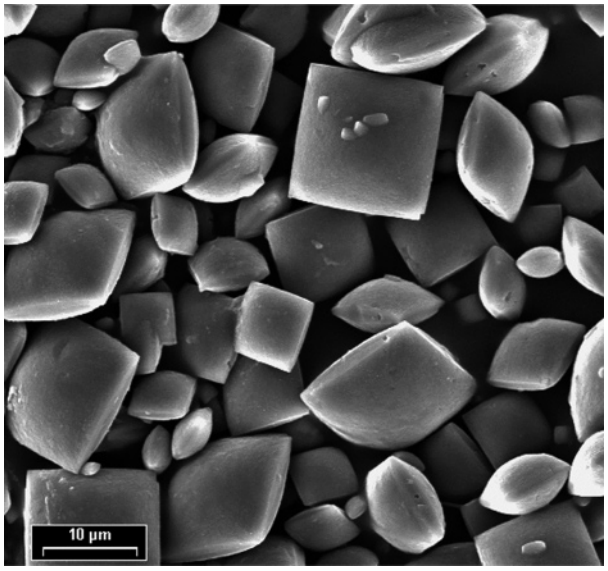

Figure 6. Scanning electron microscopy image showing the briquette-like morphology of the crystallites of SSZ-63.

Analytical Methods. Powder X-ray diffraction (XRD) patterns were recorded on a Siemens D-500 instrument. Scanning electron micrographs (SEM) were recorded on a Hitachi S-570 instrument. Transmission electron micrographs (TEM) and electron diffraction patterns were obtained with a JEOL 2010 instrument operating at an accelerating voltage of 200 kV. Samples were prepared by dispersing the crystallites on a continuous carbon film. A double-tilt goniometer stage was used to orient the crystals in the TEM. Zone axis selected area electron diffraction patterns were obtained from the edges of larger crystals as well as smaller crystalline fragments. Simulated powder X-ray diffraction patterns of faulted intergrowths were calculated with DIFFaX. Energy minimizations of the SDA within the SSZ-63 framework were performed with Cerius2 2.1[19] from MSI using the Burchart-Universal force field.[20]

All the nuclear magnetic resonance (NMR) experiments were recorded on a Bruker AVANCE 500 wide-bore spectrometer operating at 125.7 MHz for ^{13}C nuclei. The solid-state ^{13}C NMR experiments were performed using a 4-mm double resonance Bruker MAS probe. The samples were spun at magic angle at 6 kHz, and MAS spectra were recorded after applying a 6 μs $\pi/2$ pulse. The cross-polarization (CP) magic angle spinning (MAS) spectrum was collected with cross polarization from a proton using a $\pi/2$ pulse length of 5.25 μs and a contact time of 3000 μs. A relaxation delay of 4 s was sufficient to complete relaxation in the presence of both the pristine SDA and SDA occluded within zeolite. Typically, 12000−18000 scans were acquired. The spectra were referenced to tetramethylsilane at 0 ppm. The data were processed with 50 Hz line broadening. The tentative assignments of the SDA spectrum are based on literature chemical shifts from molecules with similar chemical groups. The liquid NMR spectrum was recorded for a sample dissolved in $CDCl_3$ containing TMS as an internal reference.

Elemental analyses were performed by Galbraith Laboratories (Knoxville, TN). Thermogravimetric analysis (TGA) of the as-made SSZ-63 materials was performed on a Hi-Res TGA 2950 thermogravimetric analyzer (from TA Instruments). The sample was heated in air at a heating rate of 5 °C/min for the data collection.

The pore size and void volume of calcined SSZ-63 were probed by physisorption of argon and nitrogen. Argon adsorption at −186 °C was performed using the Micromeritics ASAP 2010.

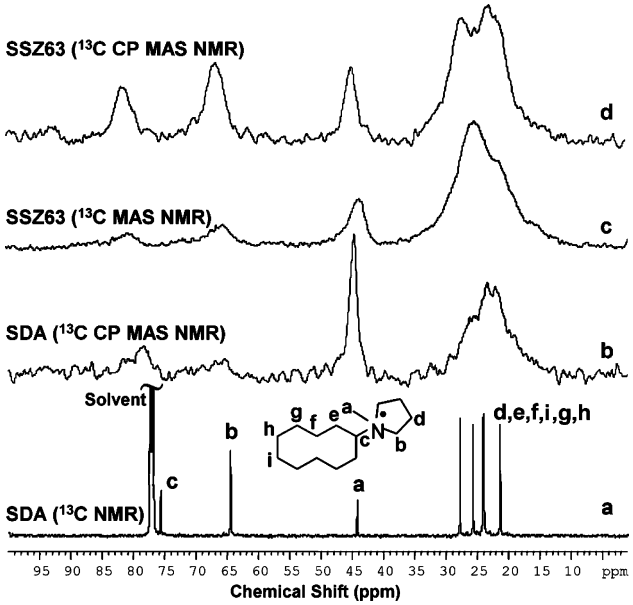

Figure 7. (a) Solution ^{13}C NMR spectrum of CDMP cation in CDCl3. (b) Solid-state ^{13}C CP MAS NMR spectrum of the CDMP in the iodide form. (c) Solid-state ^{13}C MAS NMR spectrum of the occluded SDA in an as-made sample of SSZ-63. (d) Solid-state ^{13}C CP MAS NMR spectrum of the occluded SDA in an as-made sample of SSZ-63.

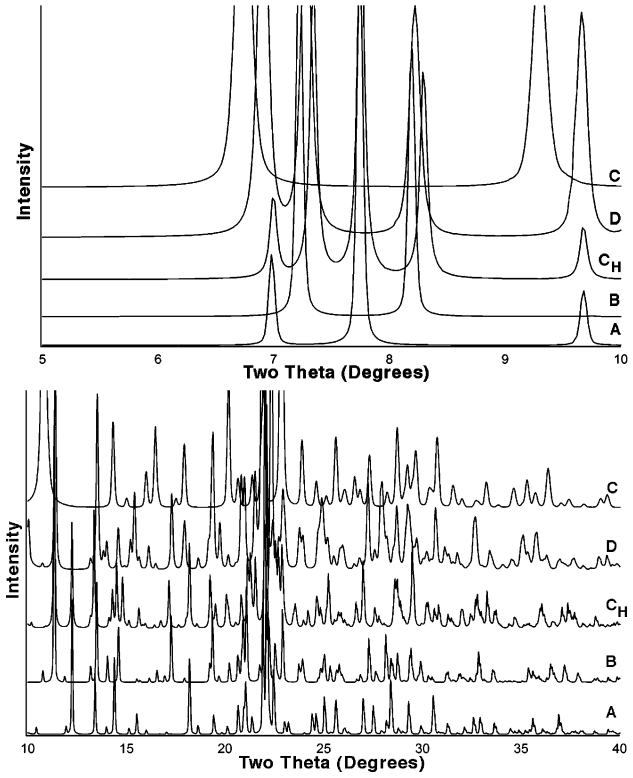

Figure 8. Simulated powder X-ray diffraction patterns of the pure polytype structures of zeolite beta (λ = 1.5418 Å).

The sample was first outgassed at 400 °C for 16 h prior to argon adsorption. The low pressure dose was 2.0 cm^3/g STP. A maximum of 1 h equilibration time per dose was used, and the total run time was 35 h.

III. Results

Synthesis. SSZ-63 was prepared using the CDMP cation (Figure 5) as a structure-directing agent in borosilicate gels.[21] The SSZ-63 sample in this study has an Si:B ratio of 39. When

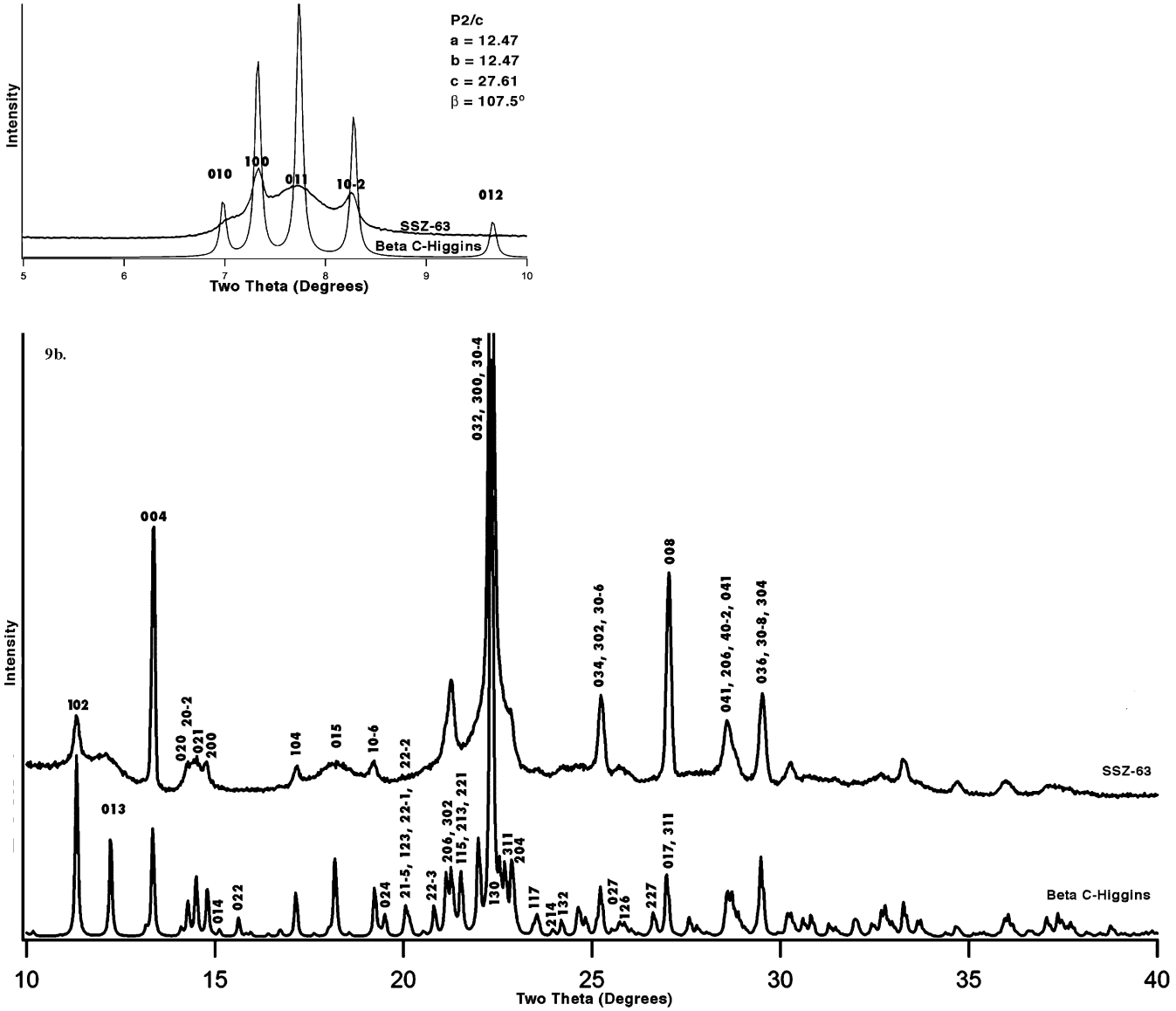

Figure 9. Comparison of the experimental powder X-ray diffraction pattern of SSZ-63 and the simulated powder X-ray diffraction pattern of polytype C_H ($\lambda = 1.5418$ Å). The *hkl* indices have been placed above their respective peaks.

aluminum is used instead of boron, zeolite beta is obtained. Unlike typical preparations of zeolite beta, the crystallites of SSZ-63 are large briquette-like crystallites that are about 5−10 μm on each edge (Figure 6). Zeolite beta samples prepared in fluoride media often possess bipyramidal crystallites that are about 10 μm in length. SSZ-63 has a micropore volume of 0.22 cm^3/g and an average pore diameter of 8.3 Å, based on an argon adsorption isotherm. SSZ-63 has a micropore volume of 0.24 cm^3/g based upon nitrogen adsorption analysis using the BET method. These micropore volumes are very close to those measured for zeolite beta. Thermogravimetric measurement of an as-made sample of SSZ-63 indicates two weight loss steps due to the loss of water and the occluded organic. The organic weight loss is 19.2%, and the water loss is 2.0%. The organic loss by TGA analysis is in excellent agreement with the organic component of 19.2 wt % determined by chemical analyses. This organic content is consistent with four SDA per unit cell of polytype A (64 T atoms). Chemical analysis of an as-made SSZ-63 indicates an atomic C:H:N molar ratio of 15.1:30.6:1, which is consistent with the ideal molecular formula of the SDA. Figure 7a shows the ^{13}C solution ($CDCl_3$) NMR spectrum and the tentative line assignments of the SDA molecule used to prepare SSZ-63. Panels b−d of Figure 7 show the solid-state ^{13}C MAS NMR spectrum of the SDA in its iodide form, the solid-state ^{13}C MAS NMR spectrum of the as-made sample of SSZ-63, and the solid-state ^{13}C CP MAS NMR of the as-made zeolite, respectively. The data indicate a good correlation between the resonances in the spectra of the raw SDA molecule and the resonances in the spectra of the as-made zeolite. The C/H/N analyses and the ^{13}C NMR data together provide definitive evidence that the SDA molecules remain intact within the framework of the zeolite sample.

Preliminary Powder X-ray Diffraction Analysis. Figure 4 compares the powder X-ray diffraction patterns of zeolite beta and SSZ-63. The patterns show very noticeable similarities as well as some striking differences. In both patterns, the *hkl* reflections for which both $h = 3n$ and $k = 3n$ are relatively sharp. Note that n does not need to be the same integer value for h and k. These peaks are sharper in SSZ-63 than they are in zeolite beta because of the larger crystallite dimensions of SSZ-63. However, there are several peaks in the pattern of SSZ-63 that are absent in the pattern of zeolite beta. The most noteworthy examples are the well-defined cluster of peaks that

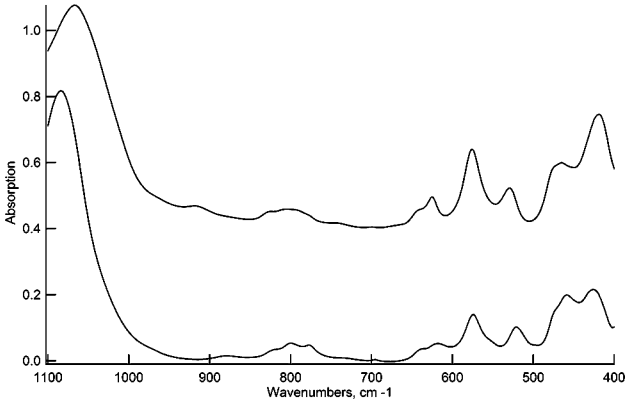

Figure 10. Infrared spectra of (bottom) calcined zeolite beta and (top) calcined SSZ-63.

occur between 6.5 and 9.0 °2θ as well as the peaks at 11.0, 17.0, and 19.5 °2θ.

The similarity of the powder pattern with that of zeolite beta suggests SSZ-63 is closely related to one of the pure beta polytypes. Comparison with the simulated traces of each of the pure beta polytypes (Figure 8) shows noteworthy similarity between the powder patterns of SSZ-63 and C_H (Figure 9a,b). In Figure 9 the *hkl* indices of C_H have been labeled above their respective peaks in the powder patterns. For reflections with $k \neq 3n$, there is significant peak broadening; in contrast, the reflections with $h \neq 3n$ and $k = 3n$ show only slight broadening (relative to sharper reflections with $h,k = 3n$). These observations imply there is a significant faulting disorder associated with translational layer shifts of $\pm^1/_3 b$; however, unlike zeolite beta, there is little stacking disorder associated with translational shifts of $\pm^1/_3 a$. This indicates that only occasional stacking disorder will be observed in the projection of C_H that corresponds to Figure 2b; in contrast, there will be significant faulting within the projection that corresponds to Figure 2a. Figure 10 shows the infrared spectra of the calcined versions of SSZ-63 and zeolite beta. The similarities in the band positions and intensities of each spectrum are consistent with the close relationship of the two structures. The differences in the spectra may be attributed to the different heteroatom species within each structure. SSZ-63 is a borosilicate, whereas zeolite beta is an aluminosilicate. Also, differences in the long-range order of the two zeolites should yield subtle variations between their spectra.

It seems strange that severe stacking disorder would be associated only with a single projection of the beta polytype. The structure-directing agent may prefer a packing arrangement that favors greater order in the zeolite framework. The cyclodecyl ring imposes a high degree of asymmetry in the atomic arrangement of the large CDMP cation. Such asymmetry would be more apt to result in preferred packing arrangements of an SDA molecule. However, we do not observe SSZ-63 when aluminum is used in the synthesis and instead conventional zeolite beta is obtained. We have observed similar behavior in the SSZ-36 system of **RTH/ITE** intergrowth structures.[15] In this example, a single SDA molecule can be used to obtain a series of zeolite phases that have varying degrees of stacking disorder. In borosilicate gels an **RTH** endmember can be produced; however, when the silica source is varied, or aluminum is used instead of boron, more heavily disordered **RTH/ITE** phases are produced. In a forthcoming publication we will discuss the effects of the gel components on the stacking disorder in the SSZ-36 system.

Molecular Modeling. We performed energy optimization calculations of the SDA within the framework structures of

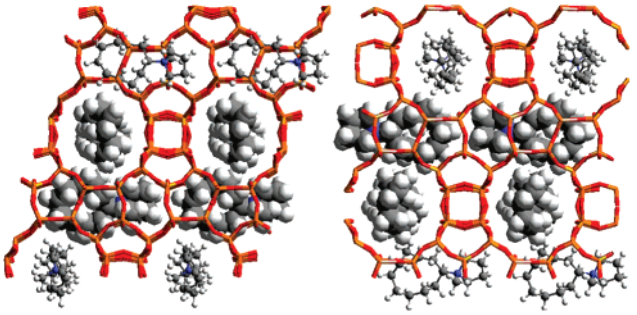

Figure 11. Energy-optimized configurations of the CDMP molecules within the framework of polytype C_H.

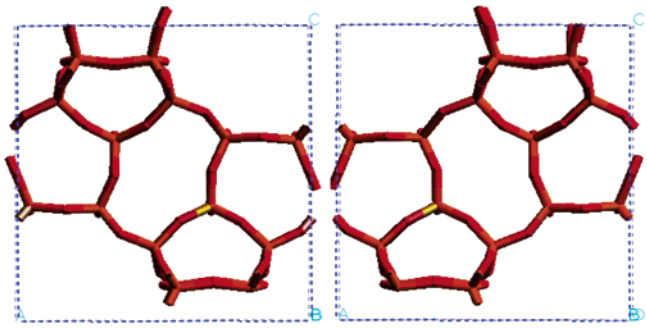

Figure 12. Layer fragments used in the DIFFaX simulations for calculations of random intergrowths of polytypes B and C_H.

polytypes A, B, and C_H. Figure 11 shows projections along the *a*-axis and along the *b*-axis of the energy-optimized configuration of the SDA molecules in the C_H framework. The illustration shows that the SDA molecules fill most of the available space within the pores. The chemical analyses are in excellent agreement with this ideal packing arrangement (1 SDA/16 T atoms. Each molecule is aligned with its long axis approximately parallel to the axis of the straight channel within which it resides. The cyclodecyl ring is located at a 12-ring window that connects neighboring pores. Within each straight channel, the SDA molecules must pack in a head-to-tail configuration in order to allow the large cyclodecyl ring to fit within a 12-ring window. All three polytype structures strongly prefer this head-to-tail arrangement. If the ordered arrangement of layers in SSZ-63 is solely due to energetic considerations of the guest−host complex, then the packing of molecules in one channel should affect the packing of molecules in its intersecting pores; i.e., van der Waals contacts between molecules in intersecting pores may affect the preferred arrangement of framework layers that optimizes those interactions. However, the optimization calculations yielded stabilization energies that varied only from −11 to −12 kJ/mol per T atom among the three pure polytypes. These values indicate a very favorable guest−host interaction compared to those we have reported earlier for SDA fits within novel framework structures. Nonetheless, we can make no clear distinction among the pure polytype structures on the basis of these energetic considerations alone. Clearly, kinetic factors play a vital role in imposing a higher degree of order in this system.

DIFFaX Simulations. To estimate the faulting probabilities of SSZ-63, we first performed a series of DIFFaX simulations in which the shifts in the *a*-direction are constant; i.e, when translational shifts in the *a*-direction are necessary, they are always in the same direction (either always $+^1/_3 a$ or always $-^1/_3 a$). On the other hand, there may be translational disorder associated with layer shifts in the *b*-direction. An example of a DIFFaX input file is shown in the Supporting Information.

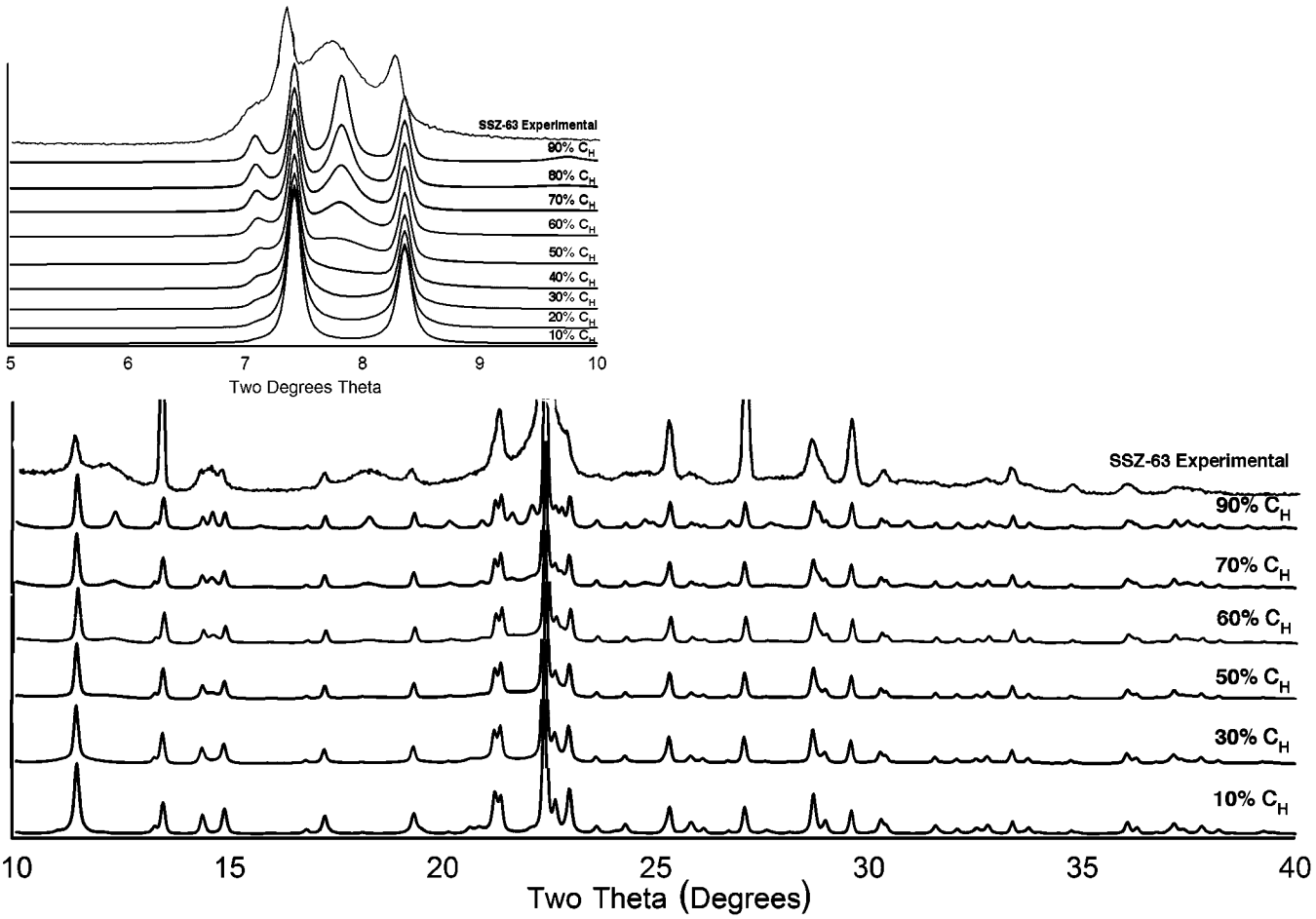

Figure 13. Simulated powder X-ray diffraction patterns of random intergrowths of polytypes B and CH ($\lambda = 1.5418$ Å). The best agreement with the experimental data is for the simulated patterns that have 60−80% C_H character.

Because it is initially assumed there is no translational disorder in every other layer, the layers used for the DIFFaX simulation are actually composed of two of the individual beta layers shown in Figure 1. Figure 12 shows two of the layer fragments used in the simulations. Equivalently, we could use the original "half-layer" types and specify the faulting probabilities such that there is no disorder caused by shifts in consecutive layers. For convenience and simplicity, we have elected to use the former route.

Polytypes B and C_H both possess the projection in the *ac* plane shown in Figure 2b. In polytype B the *bc* plane has a similar projection; however, in C_H there are alternating shifts between layers of $+{}^1/_3b$ and $-{}^1/_3b$. The *bc* projection is where we first choose to investigate the disorder in SSZ-63. We can model the disorder in this projection by defining two separate layers (Figure 12). For 100% stacking probabilities between *inequivalent* layer types, polytype C_H is obtained. For 0% stacking probability between *inequivalent* layer types, polytype B is obtained. Intermediate stacking probabilities define random intergrowths of polytypes B and C_H.

Figure 13 shows the simulated powder XRD patterns of random intergrowths of beta polytypes B and C_H. The best qualitative agreement with the experimental pattern of SSZ-63 is for 60−70% random stacking probability between inequivalent layer types. In essence, this means that SSZ-63 has approximately 60−70% C_H character. However, note that some peaks in the simulations remain relatively sharp compared to those in the experimental pattern. These peaks correspond to reflections for which $h \neq 3n$. The 102, 104, and 106 reflections are notable examples. The slight broadening of these peaks in the experimental pattern implies that the initial assumption is invalid; there is a slight degree of translational disorder associated with layer shifts parallel to the *a*-axis.

TABLE 2: Stacking Probabilities and Stacking Vectors for Layers Used in DIFFaX Simulations

layer	transition	probability	stacking vector
1	1 → 1	$(1-x)y$	$+{}^1/_3a - {}^1/_3b + 1c$
	1 → 2	xy	$+{}^1/_3a + {}^1/_3b + 1c$
	1 → 3	$(1-x)(1-y)$	$0a - {}^1/_3b + 1c$
	1 → 4	$x(1-y)$	$0a + {}^1/_3b + 1c$
2	2 → 1	xy	$+{}^1/_3a - {}^1/_3b + 1c$
	2 → 2	$(1-x)y$	$+{}^1/_3a + {}^1/_3b + 1c$
	2 → 3	$x(1-y)$	$0a - {}^1/_3b + 1c$
	2 → 4	$(1-x)(1-y)$	$0a + {}^1/_3b + 1c$
3	3 → 1	$(1-x)(1-y)$	$0a - {}^1/_3b + 1c$
	3 → 2	$x(1-y)$	$0a + {}^1/_3b + 1c$
	3 → 3	$(1-x)y$	$-{}^1/_3 - {}^1/_3b + 1c$
	3 → 4	xy	$-{}^1/_3 + {}^1/_3b + 1c$
4	4 → 1	$x(1-y)$	$0a - {}^1/_3b + 1c$
	4 → 2	$(1-x)(1-y)$	$0a + {}^1/_3b + 1c$
	4 → 3	xy	$-{}^1/_3 - {}^1/_3b + 1c$
	4 → 4	$(1-x)y$	$-{}^1/_3 + {}^1/_3b + 1c$

To account for additional disorder of layer shifts in the *a*-direction, we consider four layer types and their stacking vectors as summarized in Table 2. Layers 1 and 2 have equivalent atomic positions, and correspond to one of the layers shown in Figure 12. Likewise, layers 3 and 4 have equivalent atomic positions, and correspond to the other layer in Figure 12. Layer 1 may precede layer 1, 2, 3, or 4. In stacking from layer 1 to layer 1 or 2, the stacking direction is $+{}^1/_3a$. If layer 1 is followed by layer 1, the stacking also has a vector

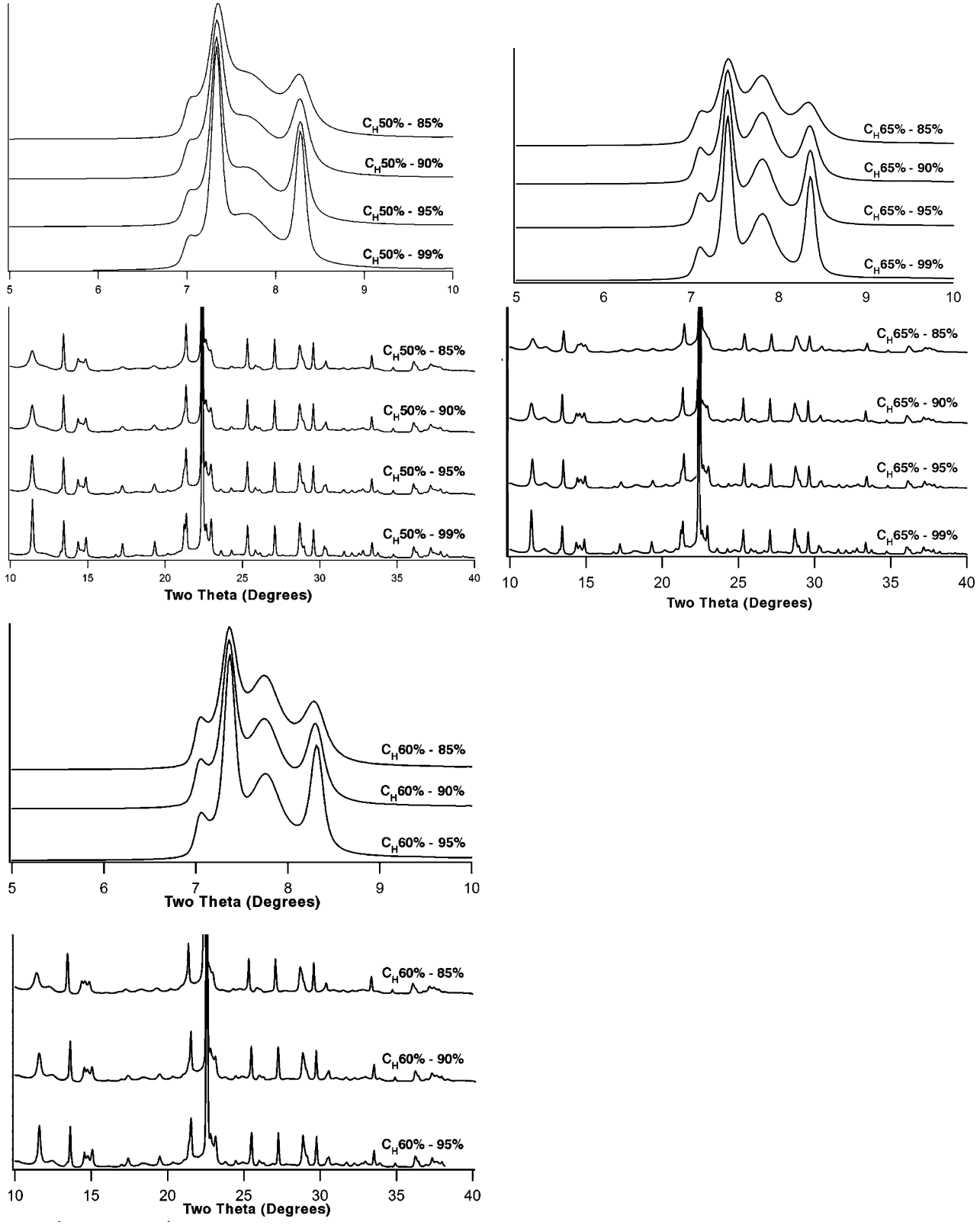

Figure 14. Simulated powder X-ray diffraction patterns for selected series of intergrowth structures having stacking disorder that arises from translational shifts in both the *a*- and *b*-directions. Each series of patterns represents a group that has the same degree of stacking disorder involving shifts in the *b*-direction.

component of $-1/3b$; in contrast, layer 2 is instead translated $+1/3b$. For stacking from layer 1 to layers 3 and 4, no translation is necessary along the *a*-direction. Again, one layer (3) will translate $-1/3b$ and the other (4) will translate $+1/3b$. Layers 1 and 2 stack to one another with a component of $-1/3a$, and layers 3 and 4 stack to one another with a component of $+1/3a$.

The sums of the probabilities of 1 → 1 and 1 → 2 (or 2 → 1 and 2 → 2) must equal the sums of the probabilities of 3 → 3 and 3 → 4 (or 4 → 3 and 4 → 4). This is equivalent to stating that the tendencies of layers to stack in the same direction as the previous layer in the sequence (when viewed along the *b*-axis) are the same. Likewise, sums of the probabilities of 1

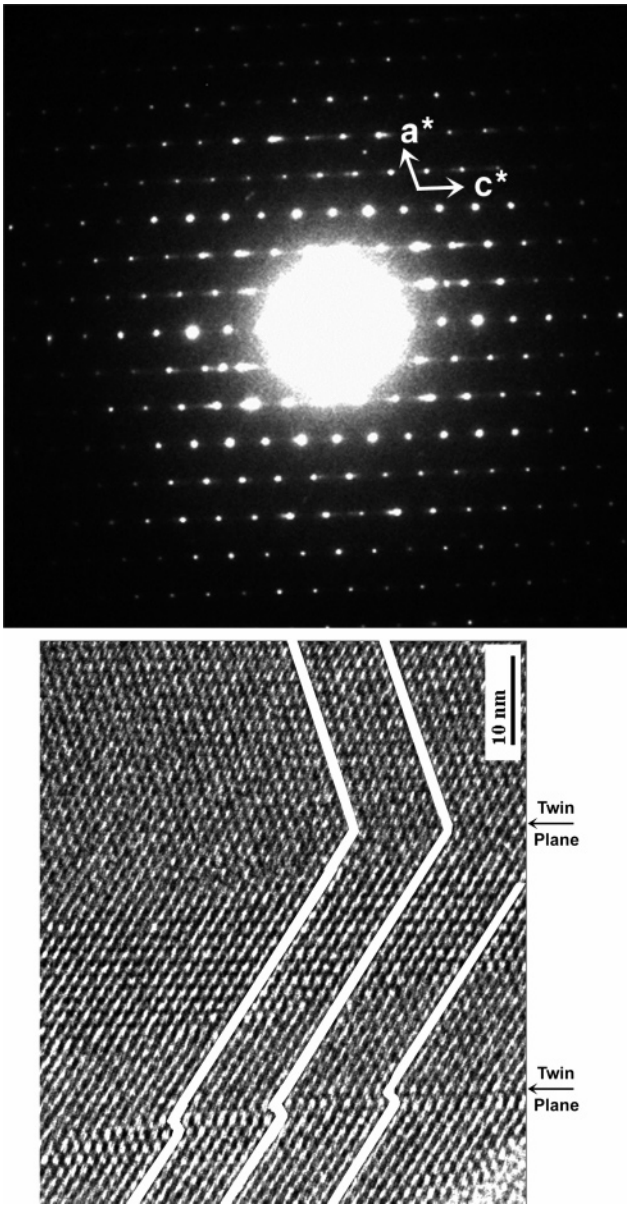

Figure 15. (a) Selected area electron diffraction pattern of SSZ-63 along the [010] zone axis and (b) the corresponding high-resolution transmission electron microscopy image. Note that in several cases the twin planes are interrupted by dislocation faults.

→ 1 and 1 → 3 must equal the sums of 2 → 2 and 2 → 4, 3 → 3 and 3 → 1, or 4 → 4 and 4 → 2. This is equivalent to stating that the tendencies of layers to stack in the same direction as the previous layer in the sequence (when viewed along the *a*-axis) are the same. The probabilities of the layers to maintain the directionality of the stacking along the *a*-direction is *y*, whereas the probability of layers to switch the directionality of the stacking along the *b*-direction is *x*. Thus the probability that a layer maintains stacking directionality along the *a*-direction and switches its directionality along the *b*-direction is the product *xy* of the probabilities.

Panels a−c of Figure 14 show series of DIFFaX simulations performed for intergrowths in which there is 50, 60, and 65% faulting within the *bc* face. Within each series, 1−15% faulting has been introduced within the *ac* face. Although all of the simulations show excellent qualitative agreement with the experimental pattern, the best matches are for patterns with 60−65% C_H character and 5−10% stacking disorder associated with layer shifts along the *a*-axis. The relative intensities of the peaks

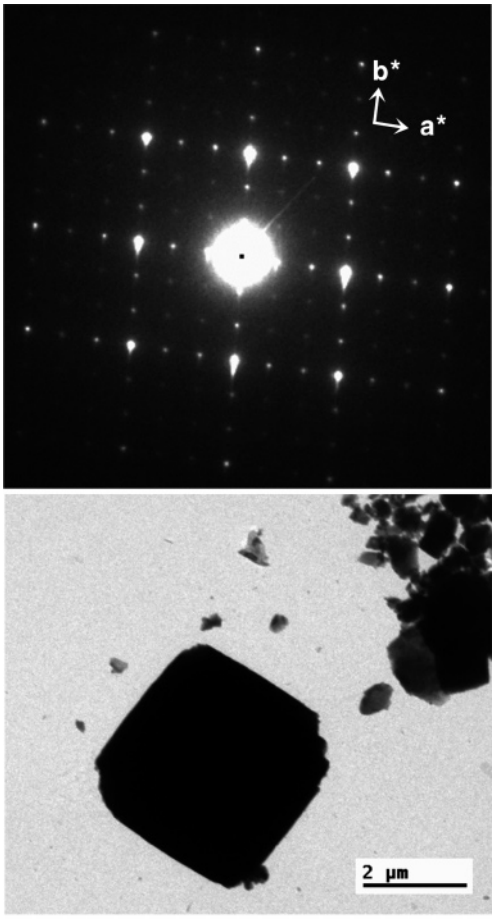

Figure 16. (a) Electron diffraction pattern of SSZ-63 along the [001] zone axis and (b) the corresponding transmission electron microscopy image.

in the low-angle cluster between 6.5 and 9 °2θ, as well as the intensities and widths for the peaks from 10 to 20 °2θ, reproduce the trends observed in the experimental pattern. There are only minor discrepancies between the simulated and experimental patterns that probably could be resolved if it were possible to refine the atomic coordinates of the layers.

Transmission Electron Microscopy and Electron Diffraction. In addition to the resemblance between the simulated and experimental powder patterns, electron diffraction data and TEM micrographs strongly support the proposed model for SSZ-63. Figure 15a shows an electron diffraction pattern along the [010] zone axis. Every third row along the *a** axis shows a series of sharp diffraction spots. The major *d* spacings in this diffraction pattern are approximately 11.8 (100) and 13.2 (001) Å, with an angle of 107°. However, there is slight streaking in the *c**-direction for the rows of the diffraction spots where $h \neq 3n$. The slight degree of streaking indicates there is occasional faulting associated with layer shifts in the *a*-direction. Figure 15b shows the corresponding HRTEM image. There are several large domains that are consistent with the stacking represented in the projection in Figure 2b, in which the layer shifts along the *a*-direction are always in the same direction. In these domains, the rows of 12-ring windows along the *a*- and *c*-directions intersect at an angle of 106°.

Striking evidence of the structural inequivalence in the *a*- and *b*-direction is observed in the electron diffraction image along the [001] zone axis (Figure 16a). Figure 16b shows the corresponding TEM micrograph. The diffraction pattern has a diamond shape because of a slight tilt away from the [001] zone axis. This was also observed in zeolite beta by Newsam and

co-workers. Note that this zone axis is perpendicular to the square projection of the crystallite. Spots located at the intersections of every third row along both a^* and b^* show strong diffraction intensities. Although the peaks for which $k \neq 3n$ are weak, the spots for which $k = 3n$ and $h \neq 3n$ possess moderate intensity. This contrasts with zeolite beta, in which no difference in intensity is observed between the *hk*0 and analogous *kh*0 reflections. Because the streaking of the diffuse reflections occurs along the c^*-direction, these peaks simply appear as weak spots when viewed along the [001] axis.

IV. Conclusions

SSZ-63 is a novel borosilicate that is related to zeolite beta. The presence of boron is required for the formation of SSZ-63 in synthesis gels using the 1-cyclodecyl-1-methylpyrrolidinium cation as a structure-directing agent. Substitution of aluminum for boron in the synthesis gels yields conventional samples of zeolite beta that possess random intergrowths of polytypes A and B in nearly equal proportions. The structure of SSZ-63 was elucidated when the similarity of its diffraction pattern with that of the polytype C_H, proposed by Higgins and co-workers, was first noted. An initial series of DIFFaX simulations showed good agreement between the experimental pattern of SSZ-63 and the simulated patterns of the random intergrowths of polytypes C_H and B that have about 60−70% polytype C_H character. This implies that, in one projection (along the [010] axis), the layers stack mostly in the same direction, while along the other projection (along the [100] axis) the stacking alternates in direction with about 60−70% probability. Additional improvement in the simulated patterns was obtained by introducing a small amount of stacking disorder (5−10%) along the [010] axis. High-resolution transmission electron images and electron diffraction data confirm the presence of the large ordered domains that are expected along the [010] axis. The simulated powder diffraction patterns, electron diffraction data, and high-resolution TEM data collectively provide strong evidence for the proposed model of SSZ-63.

Acknowledgment. We thank the ChevronTexaco Energy Technology Company, Georgie Scheuerman, and Charlie Wilson for support of our new materials research efforts. We are also grateful to Mr. Steve Trumbell for his assistance in the zeolite synthesis work, and to Mr. Kelvin Burton and Dr. E. Vittoratos for performing the adsorption measurements. We are indebted to Stacey Zones for reviewing our manuscript and providing thoughtful recommendations, and we also acknowledge Alex Kuperman for useful discussion. We also thank Kelly Harvey for her patient assistance in preparing the manuscript.

Supporting Information Available: An example of a DIFFaX input file.This material is available free of charge via the Internet at http://pubs.acs.org.

References and Notes

(1) Wadlinger, R. L.; Kerr, G. T.; Rosinskii, E. J. U.S. Patent 3308069, 1967.

(2) Lobo, R. F.; Zones, S. I.; Davis, M. E. *J. Inclusion Phenom. Mol. Recognit. Chem.* **1995**, *21*, 47−78. (b) Zones, S. I.; Nakagawa, Y.; Lee, G. S.; Chen, C. Y.; Yuen, L. T. *Microporous Mesoporous Mater.* **1998**, *21*, 199−211. (c) Tsuji, K.; Davis, M. E. *Microporous Mesoporous Mater*. **1997**, *11*, 53−64.

(3) Boggs, R. C.; Howard, D. G.; Smith, J. V.; Klein, G. L. *Am. Mineral*. **1993**, *78*, 822−826.

(4) Higgins J. B.; LaPierre, R. B.; Schlenker, J. L.; Rohrman, A. C.; Wood, J. D.; Kerr, G. T.; Rohrbaugh, W. J. *Microporous Mesoporous Mater*. **1988**, *8*, 446−452.

(5) Newsam, J. M.; Treacy, M. M. J.; Koetsier, W. T.; de Gruyter, C. B. *Proc. R. Soc. London A* **1988**, *420*, 375−405.

(6) Tomlinson, S. M.; Jackson, P. A.; Catlow, C. R. A. *Chem. Commun*. **1990**, 813.

(7) Corma, A.; Navarro, M. T.; Rey, F.; Valencia, S. *Chem. Commun*. **2001**, 1720−1721.

(8) Camblor, M. A.; Barrett, P. A.; Díaz-Cabañas, M.-J.; Villaescusa, L. A.; Puche, M.; Boix, T.; Pérez, E.; Koller, H. *Microporous Mesoporous Mater*. **2001**, *48*, 11−22.

(9) Analogous unit cells may be determined for polytypes B and C_H.

(10) Treacy, M. M. J.; Newsam, J. M.; Deem, M. W. *Proc. R. Soc. London A* **1991**, *443*, 449.

(11) Lobo, R. F.; Pan, M.; Chan, I.; Medrud, R. C.; Zones, S. I.; Davis, M. E. *J. Phys. Chem*. **1994**, *98*, 12040.

(12) Lobo, R. F.; Tsapatsis, M.; Freyhardt, C. C.; Chan, I.; Chen, C. Y.; Zones, S. I.; Davis, M. *J. Am. Chem. Soc*. **1997**, *119*, 3732−3744.

(13) Lobo, R. F.; Tsapatsis, M.; Freyhardt, C. C.; Khodabandeh, S.; Wagner, P.; Chen, C. Y.; Balkus, K. J.; Zones, S. I.; Davis, M. E. *J. Am. Chem. Soc.* **1997**, *119*, 8474−8484.

(14) Lobo, R. F.; Koningsveld, H. V. *J. Am. Chem. Soc.* **2002**, *124*, 13222−13230.

(15) Wagner, P.; Nakagawa, Y.; Lee, G. S.; Davis, M. E.; Elomari, S.; Medrud, R. C.; Zones, S. I. *J. Am. Chem. Soc.* **2000**, *122*, 263−273.

(16) Zones, S. I.; Burton, A. W. U. S. Patent 6676923 2004.

(17) Shannon, M. D. Proceedings of the 9th International Zeolite Conference, Montreal, 1992; von Ballmoos, R., Higgins, J. B., and Treacy, M. M. J., Eds.; Butterworth-Heinemann: Boston, 2003; p 389.

(18) Marler, B.; Daniels, P.; Sañé i Muné, J. *Microporous Mesoporous Mater.* **2003**, *64*(3), 185−201.

(19) Cerius^2 2.1. Product of MSI and Biosym.

(20) Rappe, A. K.; Casewit, C. J.; Colwell, K. S.; Goddard, W. A., III; Skill, W. M. *J. Am. Chem. Soc*. **1992**, *114*, 10024. (b) de Vos Burchart, E. Studies on Zeolites: Molecular Mechanics, Framework Stability and Crystal Growth. Ph.D. Thesis, Technische Universiteit Delft: Delft, The Netherlands, 2002. Table 1, Chapter XII.

(21) Elomari, S. U.S. Patent 6733742, 2004. (b) Elomari, S. U.S. Patent 6827843, 2004.